Photonics-Based Readout and Power Delivery by Light for Large-Area Monolithic Active Pixel Sensors

EIC Generic R&D for FY24

Soumyajit Mandal[1,*], Sergio Rescia[1,*], Elke Aschenauer[2], Gabriella A. Carini[1], Leo DeMino[1], Grzegorz W. Deptuch[1], Piotr Maj[1], Nicholas St John[1], and Ernst Sichtermann[3]

EIC Silicon Consortium

[1]Brookhaven National Laboratory, Instrumentation Division
[2]Brookhaven National Laboratory, Physics Deptartment
[3]Lawrence Berkeley National Laboratory, Nuclear Science Division
[*]Contact Persons, smandal@bnl.gov / sergio@bnl.gov

July 14, 2023

Abstract

This document proposes development of Monolithic Active Pixel Sensors (MAPS) read out and having power supplied by light. The scope of work is two-fold. Firstly, it addresses studies of the technology means with emphasis on implementation aspects for low-mass budget, small mechanical footprint, suitable to be located at the edges of the silicon MAPS sensors slabs, using silicon optical modulator technology and its integrability with on-sensor drivers for high-bandwidth data transmission. Secondly, it addresses investigations towards exploitation of the supply of electrically isolated power to the sensor slabs using optical power components. On the photonics side, the efforts will include 1) purchasing, bench testing, and running moderate-level radiation testing of a commercial or R&D data transfer solution at > 10 Gb/s; and 2) studying the feasibility of replacing this discrete-component solution with Si-photonics integrated on a heterogenous ASIC platform such as the GlobalFoundries (GF) 45 nm fully-depleted silicon-on-insulator (FDSOI) process with built-in optical components.

The major goals of delivering power by light include reducing the detector mass budget and ensuring a small mechanical footprint. The proposed optical power delivery modules will be suitable for being located at the edges of the silicon MAPS sensors slabs, thus providing an alternative to conventional powering over electrical cables. Advantages compared to electrical power delivery, either through direct (parallel) or stacked (serial) powering schemes, include 1) robustness to electromagnetic interference (avoiding the formation of unpredictable ground loops); 2) eliminating the need to increase the output voltage for biasing the MAPS sensor; and 3) eliminating voltage drops on power lines due to the the use of thin cables to conform with the restricted material budget of the detector. The proposed research tasks focus on purchasing, bench testing, and moderate-level radiation testing of a commercial or R&D solution to investigate the feasibility of optical power converters for the MAPS RSUs. The module will be required to supply a DC voltage suitable for generating regulated outputs at 3 V and -5 V and 15 V while delivering power in the range from 50 mW to 3 W. It will be connected to a Watt-level near-infrared laser and its associated driver and evaluation kit. The overall target of these efforts will be to either prove or disprove the utility of photovoltaic (PV) cells for optical power delivery through testing a combination of power sources with optical power converters and their packaging and housing needs. The resulting power-over-fiber (PoF) links should be able to deliver up to 3 W of electrically isolated power for powering sensor slabs in the fiducial volumes of tracking and vertexing layers for the EIC.

Follow-up activity, based on the results of this proposal, will focus on the future development of a complete solution for optical data and power delivery to the Large Area Sensors used for the EIC tracking and vertexing layers, including the outer, sagitta layers and the disks in the hadron and electron directions. The current plan for the ePIC silicon vertex tracker (SVT) layers is to directly employ the ALICE-ITS3 sensors for the innermost barrel layers, whereas the sagitta layers and end-cap wheels are to be conceptually evolved from the aforementioned ALICE-ITS3 sensors, despite the fact that their properties are not fully satisfactory for the ePIC SVT detector. The baseline solution for the EIC-specific sensors to be forked off the ALICE-ITS3 sensors endorses only minimal changes to the sensors design due to, primarily, the risk of undertaking a completely new design in the light of the need of delivering operational sensors in the restricted timeline for the construction of the EIC and its detectors. An alternative is to develop entirely new Repeated Sensor Units (RSUs) that are capable of delivering simultaneously high spatial and temporal resolution at low power consumption for upgrades of the EIC tracking and vertexing layers, during which they can be used to substitute the original RSUs used by the ALICE-ITS3 sensors. This proposal will enable the deployment of such improved RSUs, as well as reduce detector background for the existing RSUs, by providing Galvanically-isolated high-speed data and power delivery with an ultra-low materials budget.

Contents

1 Introduction

1.1 Synopsis of the R&D Proposal

Analysis of the EIC background shows that it is dominated by 1) electrons curling in the magnetic field, and 2) X-rays generated in the bremsstrahlung process. The resulting performance requirements for the inner tracking and disks layers include a timing resolution much better than 1 μs, with an optimal timing resolution on the order of 200 ns. However, this level of timing resolution significantly exceeds what is available from the ALICE-ITS3 monolithic active pixel sensors (MAPS) that will be used in these detector layers. The timing resolution achievable with the ALICE-ITS3 sensors is limited by 1) the readout of the registered hits based on a priority encoder that requires snapping of individual frames (also known as strobing), which is a legacy of the ALPIDE concept [23, 9]; and 2) by the operation of the front-end amplifier - discriminator combination, which is characterized by a significant time walk due to strict power consumption constraints. The timing resolution of the barrel layers and of the hadron and electron direction disks is also important, in fact just as important as their spatial resolution. On the other hand, for the outer, sagitta layers and further disks, the pixel pitch can be slightly larger compared to the ALICE-ITS3 sensors, leaving room for optimization of timing resolution and power consumption while staying within the limits of a 30 μm pitch. *Overall, the greater importance of high timing resolution for the EIC with respect to the ALICE ITS3 upgrade requires investment in new R&D.*

The design of the ALICE-ITS3 sensors, which are organized in almost 2 cm wide slabs stitched along their width, is modular. The sensors consist of 1) the end caps, which are used for delivery of power and I/Os; and 2) the inner frame, which provides voltage regulation, monitoring of internal functions and transmission of data to the end caps within which the Repeated Stitched Units (RSU) are embedded. Such a scheme allows substitution of the original RSU by a new block, assuming that pin-outs of the new block is compatible with the hook-ups of the inner frame. This opportunity, i.e., development of a MAPS detector with new capabilities but minimized development effort, will be explored as part of another generic R&D proposal from our team.

The main goal of this proposal is to address fundamental power and data transfer issues to the MAPS in the inner layers of the ePIC detector, which could be either the ALICE-ITS3 sensors or the improved MAPS discussed above. However, these issues are expected to even more significant for the improved high-resolution detectors, since achieving higher timing resolution will be accompanied by increases in both the power consumption and average data rate. *Specifically, the proposal will explore optical data and power links for establishing Galvanically isolated connections from the chosen MAPS to the ePIC data acquisition (DAQ) and power delivery systems, respectively.*

1.2 Physics Motivation for the ePIC SVT Detector, Detector 2, and Upgrade Needs

The need to develop technologies for reducing the materials budget (and resulting background) required to deliver resources (i.e., power, bias voltages, and data) to/from the silicon vertex tracker (SVT) detector and the DAQ system arises directly from the EIC science requirements. These requirements, which are summarized in the EIC Yellow Report [1], have been refined in later studies and are discussed below. However, we note that reducing the materials budget for resource delivery should not sacrifice its performance metrics, such as bandwidth and energy efficiency.

The key requirements for an EIC detector such as ePIC are 1) hermeticity and large rapidity coverage, $\eta \in (-4, 4)$; and 2) excellent momentum resolution for event kinematics reconstuction, jet reconstruction, jet correlations and substructure studies, and others [1]. The requirements on the vertex resolution are driven by heavy flavor reconstruction, for which reduction of the background relies strongly on analysis-related selections performed using different combinations of the primary scattering vertex and the secondary vertex of the decaying heavy meson. All these requirements

can only be fulfilled by a tracker system utilizing detectors that are highly granular, lightweight and capable of providing sub-microsecond timing resolution. Specifically, even a timing resolution on the order of $\sim 100\,\text{ns}$ would be advantageous compared to the existing detector design.

The combination of 1) a relatively low signal rate from collisions, and 2) the requirement for stringent systematic control for measurements, calls for low background and detector noise during EIC experiments. For the EIC, the background overlaid on the desired physics is dominated by 1) electron and hadron beam gas scattering in the electron and hadron directions, respectively; 2) electrons curling in the magnetic field; and 3) X-rays generated by electrons via the bremsstrahlung process. This background translates to the requirements on timing resolution being just as important as those on spatial resolution and the total material budget of the vertex and tracking layers. The latter are organized in the form of 1) the barrel layers, and 2) the hadron and electron direction disks. This vertexing and tracking system, along with the Electromagnetic Calorimeter (EmCal) and Particle Identification (PID), form the central part of the detector. These components play a crucial role in exploiting the Deep-Inelastic Scattering (DIC) process, which is the basic process at the EIC because of its unmatched precision in studying the inner structure of nuclear matter.

The total material budget located before the PWO-like EmCal and PID detectors, such as the Detector of Internally Reflected Cherenkov Light (DIRC), represent important challenges. On the one hand, it is desired, for accurate PID, to have better than 1 mrad angular resolution into the PID subsystems. On the other hand, assuming 5% efficiency loss for the electrons, the tolerable amount of material in front for the high resolution EmCal is only $\sim 5\%$ of the material-specific radiation length, X_0, assuming a certain distance of the material from the interaction point and a suitable reconstruction method. The DIRC, in particular, appears to require an angular resolution of 0.5 mrad or even better. In part, the resolution is assured by the granularity of the detector. However, from multiple scattering arguments, achieving such a resolution level in the sub $\sim 5\,\text{GeV}$ momentum range (which is interesting for the physics) is hard with inactive material present directly in front of the PID, unless this material is reduced to a total level not exceeding a few percent of X_0. Even if the latter is achieved, a significant problem of production of X-rays, resulting from the bremsstrahlung process, needs to be addressed. On the one hand, this can be handled by using 1) extremely thin detector layers, and 2) detectors that can provide improved timing resolution to improve full reconstruction of the event with high suppression of the background. However, this may not be enough, and further reduction of the material may be needed. Here the best target is seeking alternatives for any high-Z elements, which may significantly degrade X_0 even if present is small quantities. Let us assume that the vertex and tracking detector layers are made of Silicon sensor slabs that are either self-supporting or laid out on a lightweight Carbon fiber (CF) frame. A significant gain in X_0 can then be expected should delivery of resources to the sensors (i.e., power supplies, biases, and down- and up-links for data transfer) be realized in an optimal way. These resources typically utilize variants of Copper (Cu) cables (as described in more detail in the next section), with the dominant component being flex substrates with Cu traces.

Serial powering, as already proposed for the ePIC SVT detector, is an attractive first step towards realizing the desired reduction in the volume of material within which electrons can generate X-rays. The next step would be to explore elimination of the Cu cables by handling the delivery of resources by light, i.e., through optical fibers. Fibers represent only a negligible addition to the material budget as their diameters are extremely small and their material budget cost is equivalent to that of Si. Optical data and power links offer an additional positive effect by establishing Galvanically isolated connections from any chosen detector subsystem to the DAQ. Such isolated connections have multiple advantages, including 1) elimination of ground loops, 2) removing the concern of equalizing voltage levels when signals between subsystems are exchanged, and 3) increas-

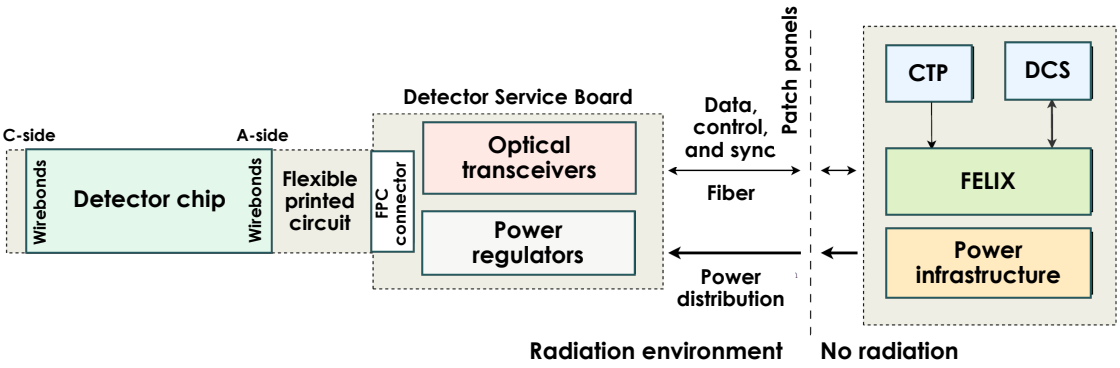

Figure 1: Overview of the ePIC silicon vertex tracker (SVT) readout services architecture. Adapted from a figure by J. Schambach, ORNL. Acronyms: CTP: Central Trigger Processor; DCS: Detector Control System; FELIX: FrontEnd LInk eXchange; FPC: Flexible Printed Circuit.

ing immunity to failures since (unlike for serial powering), each detector subsystem is individually supplied and serviced by light.

1.3 Basics of Monolithic Active Pixel Sensors (MAPS)

A Si-based tracker (SVT) system utilizing Monolithic Active Pixel Sensors (MAPS) technology [7] will be used to satisfy the material budget and spatial resolution requirements of the EIC physics program. Monolithic photon detectors integrate the sensor matrix and readout circuitry in one piece of silicon, as opposed to the hybrid approach where the sensor matrix and readout circuitry are implemented in two separate pieces of silicon [7, 15]. This approach offers multiple advantages, including easier detector assembly, lower production cost, individual pixel readout, radiation hardness, high-speed operation, low power consumption, and operation from low supply voltages [18]. MAPS wafers can also be thinned to minimize the material budget, $\epsilon = x/X_0$, of the detector, where x is the thickness of a given layer [19].

Older-generation MAPS, such as those used in the Heavy Flavor Tracker (HFT) at STAR [10] were built on low-resistivity substrates and operated in analog mode. By contrast, new inner trackers in Nuclear Physics (NP), such as the Inner Tracker System (ITS) for the ALICE experiment at the LHC (including earlier ITS1/2 designs and the current ITS3 design), utilize MAPS built on substrates with increased resistivity in the Active Sensitive Volume (ASV), managed using low detector capacitance [18, 15]. These modern MAPS detectors are operated in digital mode, thus simplifying readout. Moreover, they have been physically thinned to realize detectors that represent only a fraction of a percent of X_0 per layer [19].

2 Description of Data and Power Links for MAPS Sensors

2.1 Readout Services for the ePIC Detector

Fig. 1 summarizes the architecture of the readout services (including both data and power) envisaged for the MAPS-based SVT detector to be used by ePIC. Detector segments are organized into half-barrels. Detector outputs from each half-barrel are transmitted over copper cables (∼30 cm long) to a detector service board (DSB) for aggregation. Groups of 4 cables are fed into a VTRx+ optical transceiver chip. The VTRx+ outputs are aggregated on a single optical fiber (∼130 m long) and transmitted at 10.24 Gb/s to the counting room, which sits in a low-radiation environment.

Data on the fibers is received by the FELIX DAQ system. The latter communicates with the central trigger processor (CTP) and detector control system (DCS), both of which are also located within the control room. The CTP and DCS can send/receive control, trigger, and sync signals

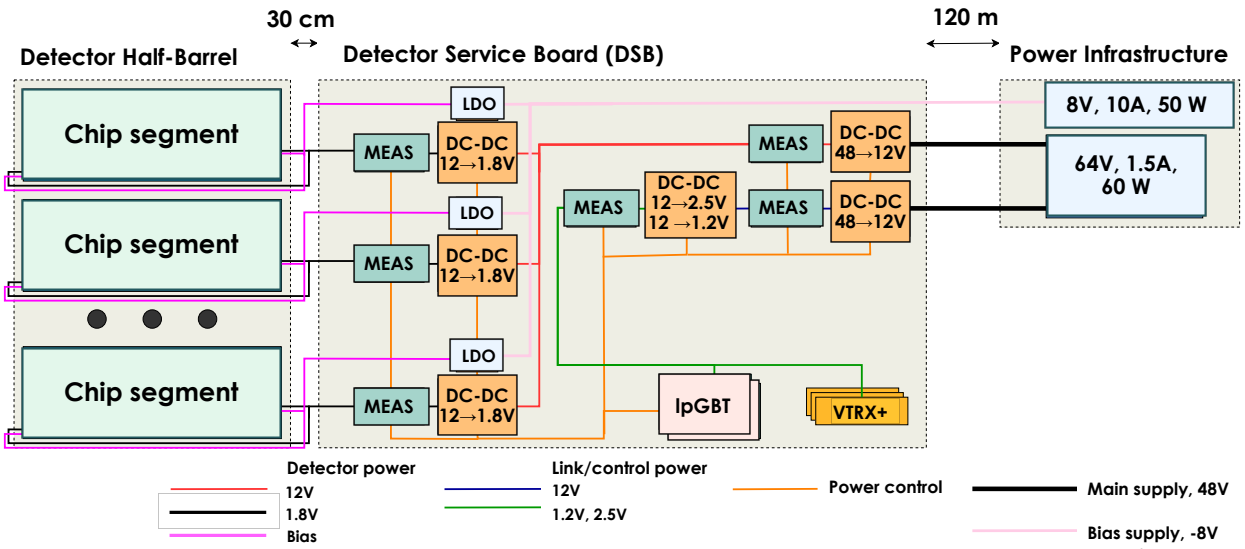

Figure 2: Overview of the power management section of the ePIC SVT readout services architecture. Adapted from a figure by J. Schambach, ORNL. Acronyms: MEAS: Measurement block, LDO: low-dropout linear regulator.

to/from the DSB via a secondary bidirectional optical fiber link (5.12 Gb/s uplink, 2.56 Gb/s downlink). An additional VTRx+ chip is used to send/receive these clock/control/trigger signals, which are relayed to the detectors by lpGBT transceiver chips over additional ∼30 cm long copper cables (e-links) running at 40 Mb/s. The lpGBT chips also provide slow control signals to the detectors over the same e-links.

Fig. 2 shows the power management section of the SVT readout services in more detail. The design operates off two main DC power supplies located in the counting room: 48V for the DSBs and detectors (set to a relatively high value to minimize I^2R loss on the cables), and −8V for the detector bias voltages. Both supplies are fed to the detector via copper cables. The 48V supply is converted to 12V/1.8V (for the detectors) and 12V/2.5V (for the DSBs) via a set of switching DC-DC converters. By contrast, the −8V supply, which draws little current, is converted to the required bias voltage (in the −6V to 0V range) via low-dropout linear regulators (LDOs).

One challenge of the power management scheme shown in Fig. 2 is load balancing (to avoid skewed voltage drops) when both the A- and C-sides of the detectors are supplied by independent voltage sources to reduce in-sensor IR drops. Another issue is the large number of copper cables (two per detector chip), which adds to the overall materials budget of the SVT. As mentioned in the previous section, an alternative power management scheme, namely serial powering, has been proposed to reduce the total volume of copper cables. In this approach, a set of detectors (e.g., all the detectors in a half-barrel) is connected in series from a single high-voltage (HV) supply. However, this scheme requires each detector to be powered by a complex floating shunt regulator circuit, which in turn increases the overall design complexity of the power supply network.

2.2 Grounding and Power Distribution

Let us consider the problem of supplying DC power to the SVT more holistically. Large-scale particle detectors have three key features that are in conflict with high-performance electronics design. Firstly, the primary input signals to be amplified and recorded are generally very small. Secondly, the detectors cover large surface areas and are thus vulnerable to interference from external electromagnetic (EM) fields [3]. Finally, the detectors require large-scale power supply networks. The latter carry ground currents, which can generate additional EM interference (EMI)

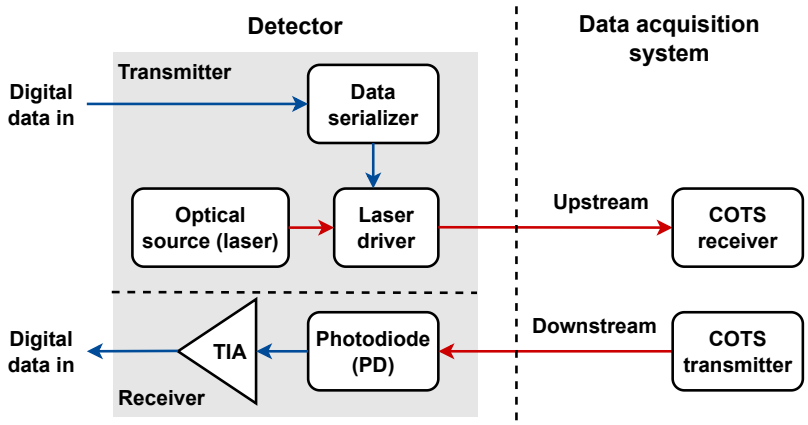

Figure 3: Block diagram of a conventional bidirectional optical data link for use in detectors.

by coupling into the signal paths (which are generally single-ended, at least within the front-end). As might be expected, poor grounding choices have indeed been found to cause significant noise problems in many high-energy and nuclear physics experiments [5]. Unfortunately, these problems often do not occur during the design phase of a detector system. Instead, they only show up when the entire system is installed and operating in its intended environment.

A common grounding philosophy within major detectors, such as LHCb, is to create a low-impedance mesh structure [3], as opposed to a classical single-point or "star" ground [12]. The use of such a mesh minimizes the areas of any ground loops. Its low impedance also 1) generates a well-defined reference voltage (i.e., an equipotential) for the entire system, and 2) forces ground loop currents to circulate within the mesh rather than being injected into other nodes. Nevertheless, the problem of ensuring EM compatibility (EMC) for the detector front-ends remains a significant design challenge. The large conductor volume required to generate a suitably low-impedance ground mesh can also significantly increase the detector's materials budget and background level.

2.3 Optical Data Links

EMI/EMC problems can be significantly reduced by using Galvanic isolation to break ground loops. For example, communications between counting rooms and detectors at the LHC are almost exclusively over optical fibers, which provide Galvanic isolation while also 1) being more compact than electrical cables, and 2) providing higher bandwidth [20]. Similar fiber data links are envisaged for the ePIC SVT, as shown in Fig. 1. Fig. 3 shows a block diagram of such conventional optical data links (a bidirectional version is shown for completeness). Early LHC detectors used optical link systems constructed using both commercial off-the-shelf (COTS) components that were tested to be radiation tolerant (such as the G-Link chip-set) [2] and custom ASICs developed by CERN (such as the GOL serializer) [13]. Transmission speeds ranged from 80 Mb/s to 1.6 Gb/s per fiber. Later solutions replaced the on-detector side of the link with ASICs to enable performance improvements (higher data rate and radiation tolerance) within a limited power budget. The Phase-I upgrades to the LHC detectors increased data rates to ∼5 Gb/s per fiber [14]. Ongoing Phase-II upgrades for the HL-LHC will further increase rates to ∼10 Gb/s per fiber [22] by using the CERN-developed lpGBT transceiver ASIC, which can operate at 10.24 Gb/s. The corresponding optical modules have also been fully customized to meet dimension, channel density, and radiation/$\vec{B}$-field tolerance requirements, as originally identified during the CERN-led *Versatile Link* project. The designs, including VTRx and MTRx, use vertical-cavity surface-emitting lasers (VCSELs) as electrical-optical converters and radiation-tolerant multi-mode fibers with a nominal length of 150 m.

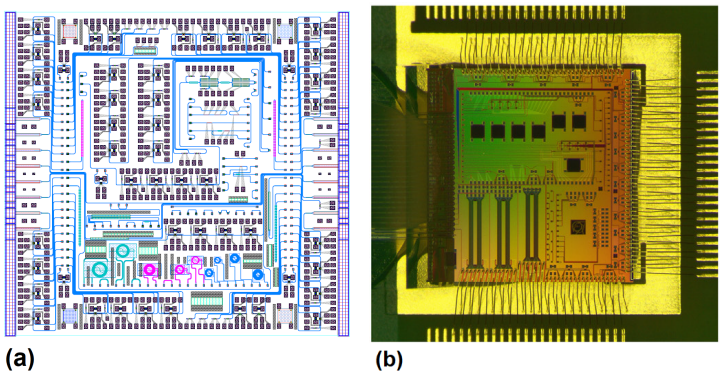

Figure 4: (a) Layout of the CERN PICV3 photonic IC (PIC), and (b) die photograph the CERN PICV2 chip [16]. Both PICs measure 5×5 mm^2 and were fabricated through a multi-project wafer (MPW) service.

Commercial short-range (∼100 m) optical links, which are not constrained to be radiation tolerant and often have less strict power dissipation requirements, have reached much higher data rates. The use of fast electro-optic modulators (EOMs) and spectrally-efficient communication schemes such as PAM4 have enabled data rates of $>$ 56 Gb/s per fiber with high energy efficiency ($<$ 30 pJ/bit). Data rates can be further increased either electronically (e.g., by using faster serializer circuits) or optically (e.g., by using wavelength division multiplexing [WDM], spatial division multiplexing [SDM], or polarization division multiplexing [PDM]). A major goal of the proposed project is to demonstrate such energy-efficient high-data-rate links within a transmitter footprint that is suitable for integration within the ePIC SVT detector. Specifically, the goal is to miniaturize the optical data module such that it fits within part of the flexible printed circuit board (PCB) connecting the detector chips to their local DSB (see Fig. 1), thus eliminating all electrical data links (e-links) between the MAPS and the control room.

3 Proposed Optical Data Links

3.1 Link Architecture

The key electrical-to-optical conversion step of an optical data transmitter can be implemented using either 1) a separate optical module (the COTS solution); or 2) a custom Si-based photonic integrated circuit (PIC). A key advantage of the latter approach is integration of high-speed electrical circuits (using CMOS transistors) with optical components within the same wafer, thus eliminating the need for high-bandwidth connections between the chip and a separate optical module. Fig. 4(a) shows the layout of a modern PIC designed for data readout from high-energy physics (HEP) detectors. The chip contains four electro-optic modulators (EOM) and a 4× WDM to multiplex their outputs. The four wavelengths can span either of the two common optical communications bands, namely O-band (1310 nm) and C-band (1510 nm). Fig. 4(b) shows a die photograph of an earlier version of the same design after wirebonding of the electrical connections [16, 21].

Fig. 5 shows an overview of the proposed optical data link architecture. While a bidirectional version is shown for completeness, this project will focus on the upstream (detector → data acquisition system) side of the link. Compared to the conventional architecture shown in Fig. 3, the proposed architecture minimizes on-detector area, power consumption, and cooling requirements by moving the optical source (a CW laser) to the DAQ end of the link [16]. Instead, the laser light is modulated using an EOM integrated within a PIC along with a high-speed data serializer. A variety of EOM designs are possible. Their relative advantages and disadvantages are summarized in Table 1. This project will focus on interference-based modulators (MZMs) and resonator-based

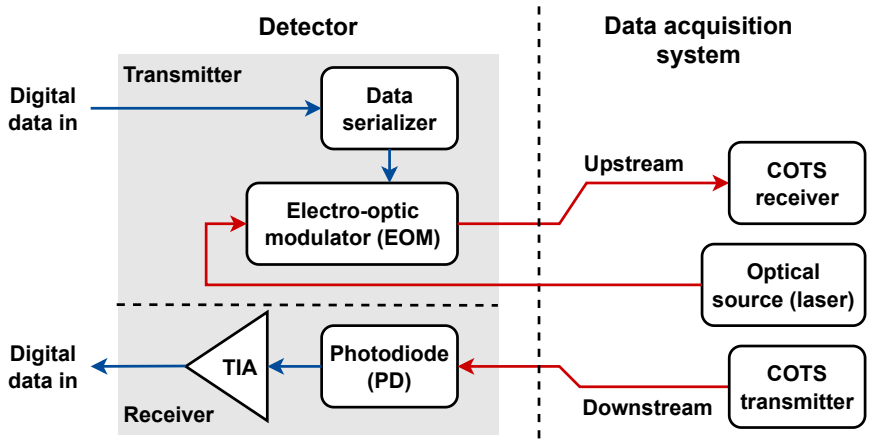

Figure 5: Block diagram of a bidirectional version of the proposed optical data link for ePIC and later EIC detectors.

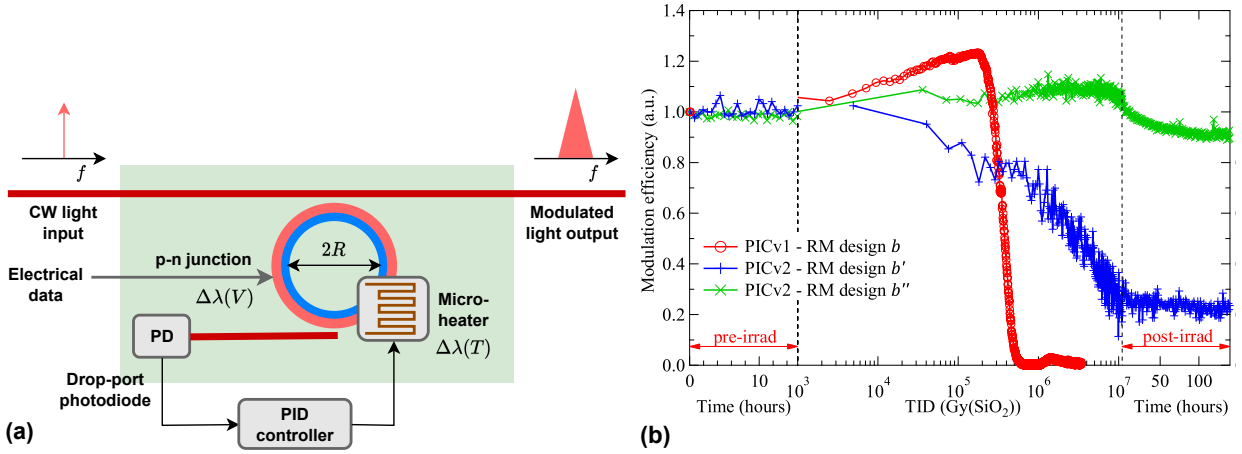

Figure 6: (a) Design of a practical ring modulator (RM) with built-in temperature tuning to ensure stability of the resonant frequency versus temperature. (b) Effect of radiation on modulation efficiency of RMs fabricated on three PIC designs, showing that tolerance to high levels of radiation is possible by careful design [21].

modulators (RMs) due to their availability as mature components within the process development kit (PDK). We will evaluate the relative benefits of the two topologies, including size and temperature sensitivity. The high temperature sensitivity of RMs requires either precise wavelength control or automated tuning via a built-in heater and thermal controller, as shown in Fig. 6. On the other hand, conventional MZMs use traveling-wave delays as phase shifters, resulting in relatively large device footprints. Lumped-element versions of MZMs can be used to reduce the device footprint and power consumption while improving high-speed performance [6].

Given the high-radiation environment of the ePIC detector, it is important to verify that the proposed PIC-based optical data links are radiation-tolerant. Fortunately, Si-based PICs are generally suitable for high-radiation environments [21]. Extensive radiation testing of Si-based MZMs [11] and RMs has been carried out by CERN and other organizations. Testing has focused on the total ionization dose (TID), since single-event upsets (SEUs) are expected to be a relatively small problem for PICs. This is because PICs are typically implemented in silicon-on-insulator (SOI) processes, which feature a thin bulk layer that minimizes the cross section for charge generation during single-event transients. The typical degradation mechanism (whose rate depends on the process and design parameters) is a gradual loss of modulation efficiency due to the pinch-off effects of holes

Table 1: Relative advantages of different electro-optic modulators (EOMs)

Modulator type	Advantages	Disadvantages
Mach-Zehnder Modulator (MZM)	• Temperature insensitive	• Typically, big footprint (∼1 mm) and high modulation voltage (∼2 V) • Requires folding to reduce footprint (∼0.5 mm)
Ring Modulator (RM)	• Intrinsically much smaller than MZMs • Low drive voltage and power consumption	• Size limited in practice to ∼100 μm by pad pitch • Temperature sensitive
Ge-Si Electro-Absorption (EA)	• Compact, high speed	• More suitable for 1550 nm wavelengths
Thin-film LiNb on SOI waveguide	• High speed (40 Gb/s for 2 mm long devices at 1.4V)	• Still in early R&D phase

generated (and then trapped) in p-doped regions. The measured modulation efficiency of RMs on two PICs designed by CERN (PICV1 and PICV2) versus TID is summarized in Fig. 6.(b) [21]. These results (which are similar for MZMs) show that 1) modulation efficiency can be maintained to within ±20% for TID levels up to ∼1 MGy (∼100 Mrad) at typical operating temperatures; and 2) post-irradiation annealing (e.g., using on-chip heaters or by applying a forward current to the MZMs) results in almost immediate and complete device recovery by driving away the trapped holes. In addition, design and process optimization (e.g., higher doping concentrations or thicker etch depths) can further increase radiation resistance.

3.2 Integrated Silicon Photonics

Low-cost multi-project wafer (MPW) access to a variety of PIC processes is now available through several vendors. We plan to use the GlobalFoundries (GF) 45SPCLO Silicon-Photonics process for this purpose due to its 1) library of high-performance photonic components, 2) tight integration with a base CMOS electronics platform, and 3) domestic fabrication (in Malta, NY). The 45SPCLO process is a 45 nm generation, silicon-on-insulator (SOI) CMOS technology that supports both electronic and photonic designs [17]. Monolithic integration of RF, digital and Si-Photonic circuits results in higher energy efficiency (bits/W) and modulation rates than COTS solution. As a result, the process is widely used in applications such as automotive Lidar, high-speed networking, artificial intelligence (AI) processing, and the internet of things (IoT). Our team at Brookhaven National Laboratory (BNL) is in the process of getting multi-project wafer (MPW) access to this process through the Trusted Access Program Office (TAPO) of the Defense Microelectronics Activity (DMEA), which is run by the U.S. Department of Defense (DoD).

Fig. 7(a) shows a cross-section of the front- and middle-end of line (FEOL/MEOL) segments of the GF 45SPCLO process. The process starts with a high-resistivity silicon substrate. All components are fabricated on top of a 2 μm thick insulating layer (known as buried oxide [BOX]) deposited on the resistive substrate. The main electrical components include NFETs and PFETs

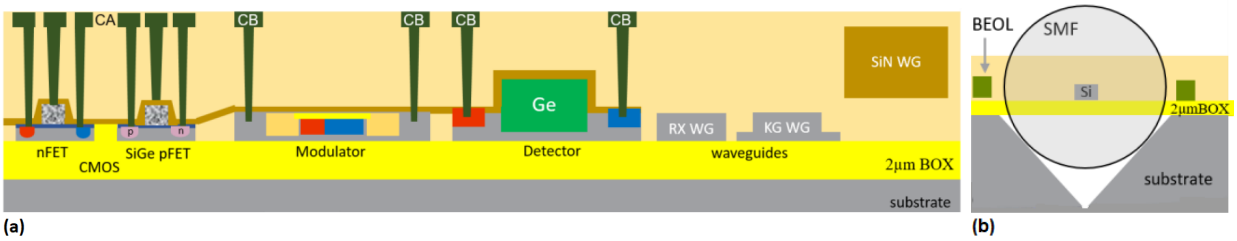

Figure 7: Cross-sections of (a) the front- and middle-end of line (FEOL/MEOL) technology, and (b) the edge coupling module used in the GF 45SPCLO process. Acronyms: CA: Active area contact, CB: gate contact, WG: Waveguide, BOX: Buried oxide, SMF: single-mode optical fiber. Figures adapted from [17].

(shown in the figure) as well as auxiliary devices (resistors, capacitors, inductors, and diodes) and 8 metal layers for interconnect (7 copper and 1 aluminum, including two 1.2 μm-thick layers). The main optical components are low-loss SOI waveguides (fabricated using SiN), ridge and slab waveguides (RX and KG, respectively), high-speed optical detectors (Ge photodiodes), and electro-optic modulators (EOMs). Waveguide losses in the O-band are ~1.4 dB/cm and ~0.4 dB/cm for the RX/KG and SiN waveguides, respectively. Both the photodiode (PD) and EOMs are designed to support data rates up to 56 GS/s, and the PD dark current is < 40 nA. Efforts to further increase data rates (e.g., by optimizing the EOM designs) are also underway [17].

High-performance optical couplers, i.e., low-loss input/output (IO) interfaces between optical fibers and on-chip waveguides, are another critical component of PIC-based optical signal processors. The 45SPCLO process features both vertical (grating) and edge couplers. The latter features a self-aligned V-groove and spot size converter, as illustrated in Fig. 7(b), with relatively low coupling loss (0.8 dB/1.5 dB in TE and TM modes, respectively). The availability of device models and their integration into computer-aided design (CAD) tools is another important factor in choosing a PIC process, since the quality of the process design kit (PDK) containing these models has a significant impact on overall PIC design time. The 45SPCLO process is well-equipped in this regard: the associated PDK includes both a standard electronic element library (FETs, precision resistors, capacitors, inductors, electrostatic discharge (ESD) protection diodes, etc.) and an extensive photonic element library (polarization splitter and rotator, modulators, photodiodes, phase shifter, waveguides, edge coupler, grating coupler, etc.). The latter are designed to operate in both the C-band (1550 nm) and O-band (1310 nm), with support for the L-band (1595 nm) underway.

4 Proposed Optical Power Links

4.1 Link Architecture

Replacing the DC power supply network with optical fibers can further reduce the potential for ground loops and power-line interference to impact detector operation. COTS solutions for optical power delivery are now available. The development of these modules has been driven by the need to deliver electrical power in applications that require complete Galvanic isolation within demanding industrial environments (e.g., factories). For example, the Broadcom AFBR-POC306A1 optical power converter, shown in Fig. 8(a), is designed to power electronic circuits in applications where using electrical wires is not feasible due to high voltage (HV), electromagnetic interference (EMI), or strong magnetic fields. The device uses a multi-junction photovoltaic cell based upon a III-V semiconductor (likely InP, GaAs, or InGaAs) that is optimized for near-infrared (NIR) operation in the 800-830 nm wavelength range. The module is reasonably compact ($10.4 \times 14.7 \times 8.2$ mm excluding the optical connector), and its volume can be further reduced by optimizing the packaging (e.g., by purchasing bare dies from the manufacturer and then developing custom encapsulation).

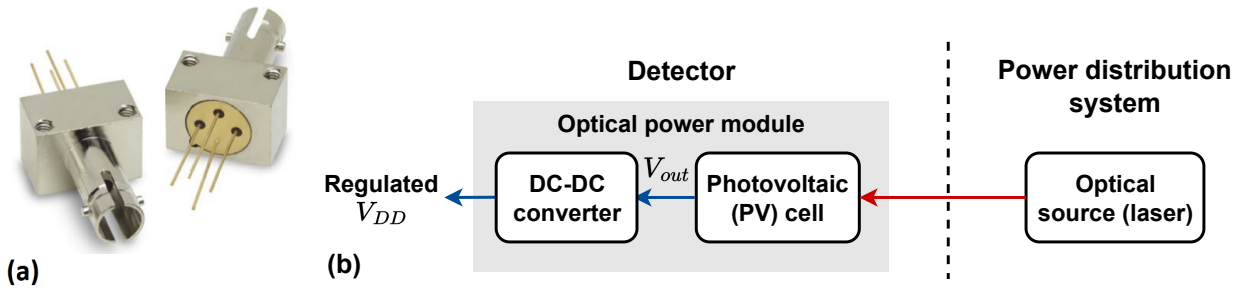

Figure 8: (a) Photograph of the Broadcom AFBR-POC306A1 optical power converter. (b) Overview of the proposed optical power link architecture.

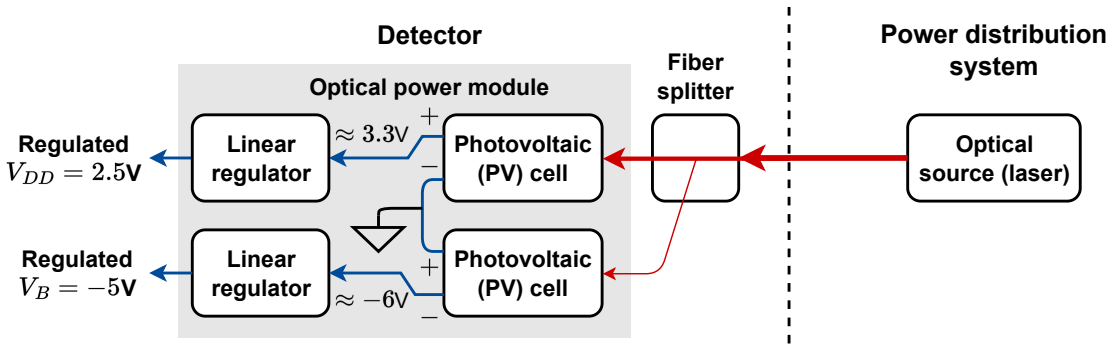

Figure 9: Modified optical power link architecture. Two independent PV modules are used to generate a split DC power supply for both powering and biasing RSUs.

Fig. 8 shows an overview of the proposed optical power link architecture. The remote optical source (a CW laser) transmits power over an optical fiber to a photovoltaic (PV) cell within the detector. The unregulated DC output voltage, V_{out}, of the PV cell, is converted into a regulated supply voltage (V_{DD}) by a DC-DC converter. The latter can be either a COTS device or an ASIC. Note that V_{out} is a truly floating voltage source (similar to a battery), i.e., is Galvanically isolated from all other electrical potentials. Thus, it can be easily used to generate the negative bias voltage, V_B, required by the MAPS. For this purpose, the light input is split (using an asymmetric fiber splitter) and fed into two independent PV cells to generate a split DC power supply, as shown in Fig. 9. The first PV cell generates the high-current output required to run the RSU (typically at +3 V), while the second generates approximately −5 V to bias the RSU substrate. The two supplies share the ground terminal, i.e., are stacked in series like batteries. Note that the negative supply has to generate little power since V_B draws a very small current compared to the RSU itself. Thus, the light output is split asymmetrically, with the bulk going to the first PV cell. The unregulated outputs of the two cells can be regulated by either switching or linear DC-DC converters, i.e., either a buck converter or a linear voltage regulator (LDO). Notice the simplicity of this design compared to the complex copper-based power management system envisaged by the current ePIC SVT detector architecture (Fig. 2).

The optical power link typically uses a multi-mode fiber to 1) allow higher optical power levels to be transmitted (due to their much larger core diameter compared to single-mode fiber); and 2) reduce cost. By contrast, the optical data links described in the previous section generally use single-mode fiber to maximize the bandwidth-distance product.

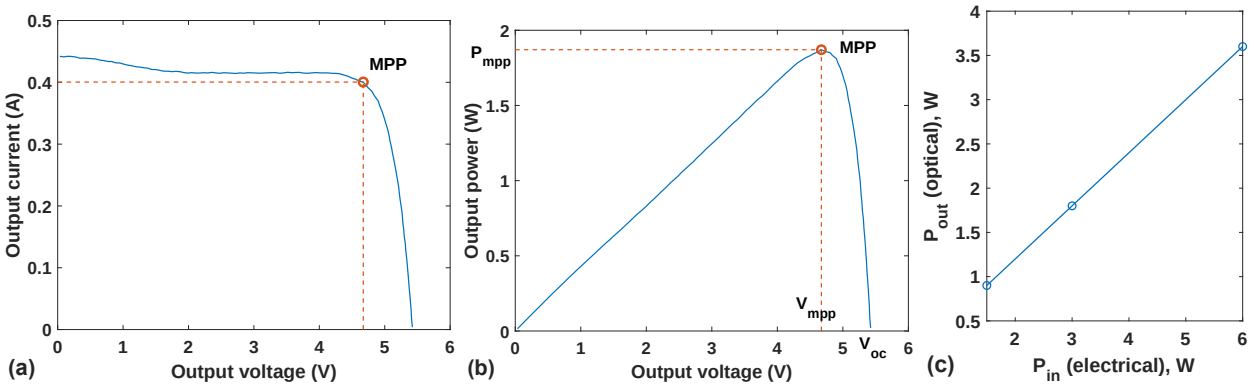

Figure 10: (a)-(b) Typical load characteristics of an optical power module: (a) output current versus output voltage, and (b) output power versus output voltage. (c) Measured power efficiency curve of the Broadcom AFBR-POC306A1 optical power converter, showing a nearly constant efficiency of $\eta \approx 60\%$.

4.2 Link Optimization

Fig. 10(a) shows the typical output voltage versus current (I_{out}-V_{out}) characteristics of an optical power converter. The maximum current is generated when the module is short-circuited, i.e., the output voltage, V_L, is zero. This is known as the short-circuit current, I_{sc}. Similarly, the maximum voltage is generated when the module is open-circuited, i.e., the output current, I_L, is zero. This is known as the open-circuit voltage, V_{oc}. The maximum power point (MPP) occurs when the output voltage drops to a value $V_{mpp} \approx 0.8 \times V_{oc}$, as shown in Fig. 10(b).

One common issue with photovoltaic devices is their light-dependent output impedance, R_s, which shows up as a shift in the I_{out}-V_{out} characteristics shown in Fig. 10(a). Maximum power delivery to the load, R_L (assumed to be resistive), occurs when $R_s = R_L$. Thus, maximizing power delivery requires R_L to be adjusted with light level, which is known as maximum power point tracking (MPPT). A variety of MPPT algorithms have been proposed for photovoltaic systems [8, 4]. The simplest MPPT algorithm is to adjust the output voltage to a constant fraction of V_{oc}, i.e., set $V_{out} = \alpha V_{oc}$ with a typical value of $\alpha = 0.75 - 0.8$ (see Fig. 10(a) for an example). Alternatives include the perturb-and-observe (P & O) algorithm, in which the output voltage is perturbed and the resulting change in output power, ΔP_{out}, recorded. The ratio $\Delta P_{out}/\Delta V_{out}$ provides an approximation of the local gradient of the P_{out}-V_{out} curve. The controller uses this information for simple gradient ascent (i.e., hill-climbing) to find the MPP.

When operated close to their MPP, the Broadcom optical power modules provide an end-to-end power efficiency of ∼60%, as shown in Fig. 10(c). This level of efficiency is similar to that achieved by conventional non-isolated power distribution networks. In addition, output power is nearly constant (within ±10%) over the industrial temperature range (−40°C to 85°C).

5 Project Realization Methodology

The proposed list of project tasks is described below. **Tasks 1-3** have the highest priority, while **Tasks 4-6** have lower priority. **Task 7** is a stretch goal that shall be undertaken if time permits.

Task 1: Development and testing of a flexible printed circuit board (PCB) to hold the COTS optical components in a form factor compatible with deployment at the ends of the ePIC staves, i.e., between the detector chips and their local detector service board (DSB) as shown in Fig. 1. The PCB will be designed to include both COTS optical data and power modules. It will be attached to single- and multi-mode fibers of different lengths during testing. The tests will include the design and verification of MPPT algorithms for the optical power link.

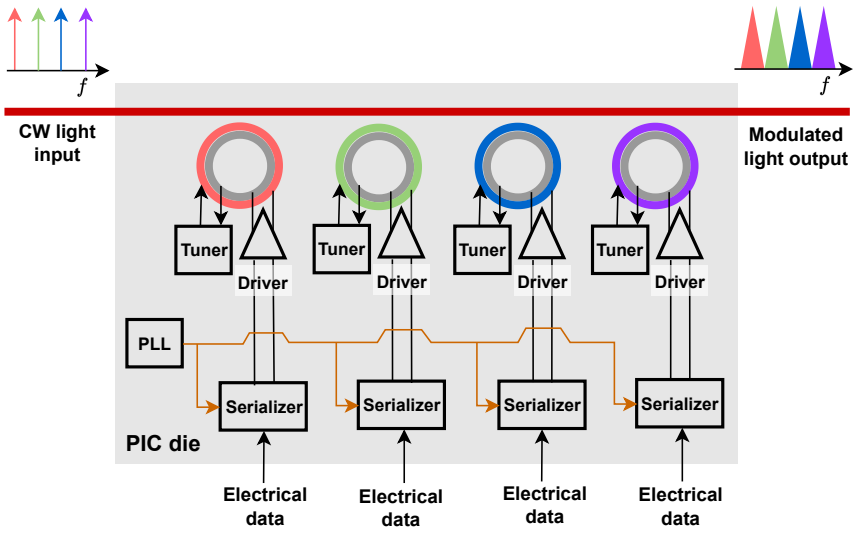

Figure 11: Block diagram of a 4× multiplexed EOM using RMs and wavelength-division multiplexing (WDM).

Task 2: Testing the radiation hardness of the COTS modulator and power-over-fiber (PoF) modules using a suitable radiation source. Specifically, we plan to use a ^{60}Co source, which is a strong γ-ray emitter ($E \approx 1.3$ MeV) and widely used for radiation testing of electronics. The goal is to 1) expose the flexible PCB containing the optical modules (Task 1) to a total ionizing dose (TID) in the 10-100 Mrad range, in line with the maximum expected TID for the ePIC detector; and 2) characterize changes in key performance parameters (including eye diagrams, maximum data rates, peak power output, and power efficiency). The testing can either be performed in-house at BNL or at the beam line at Massachusetts General Hospital (MGH) in Boston based on pricing and availability. Completing this test campaign is particularly important for the optical power modules since they have, to the best of our knowledge, never been radiation tested.

Task 3: One of the potential challenges with the proposed data and power delivery approach is interference with the MAPS due to light leakage from the optical modules. The goals of this task are to 1) experimentally measure the leakage levels using an integrating sphere; and 2) evaluate their potential impact on MAPS dark current rates via TCAD device modeling.

Task 4: Following initial verification of the proposed concept using a COTS optical module (Tasks 1-3), the next few tasks focus on gaining familiarity with the GF 45SPCLO process to enable future development of a miniaturized PIC-based version of the optical data module, as shown in Fig. 5. The specific goals of Task 4 include 1) validating the CAD flow (based on Cadence tools available at BNL) for simulating optical components included in the 45SPCLO PDK; 2) using this flow to design and simulate both MZM-based and RM-based EOMs using parametrized components (p-cells) from the 45SPCLO PDK for operation in either the C-band or the O-band; and 3) compare their relative performance using key metrics such as power consumption, modulation bandwidth, temperature sensitivity, and layout area.

Task 5: This task builds upon Task 4 by evaluating the feasibility of using multiple on-chip EOMs to implement WDM for further increasing the data rate. A set of RMs (based on the designs in Task 4) will be connected in series for this purpose, as shown in Fig. 11.

Task 6: This task focuses on evaluating the performance of the optical coupler modules available in the 45SPCLO PDK. The specific goal is to simulate the insertion loss and optical return loss (ORL) of both the vertical and lateral couplers for 1) different optical polarizations (TE, TM);

Table 2: Proposed project timeline

Month	Task 1	Task 2	Task 3	Task 4	Task 5	Task 6	Task 7
1							
2							
3							
4							
5							
6							
7							
8							
9							
10							
11							
12							

and 2) different wavelengths (C-band and O-band). The results will be used to constrain future system-level designs of PIC-based optical data modules.

Task 7 (stretch goal): The earlier tasks have focused on ensuring Galvanic isolation for both the high-speed data and power links used by the SVT detector chips. However, ensuring complete isolation also requires the slow control links (see Fig. 1) to be redesigned. This goal can obviously be achieved by simply adding a third, low-data-rate, optical link in parallel with the other links. However, this approach may be undesirable due to the proliferation of optical fibers. Instead, this task will explore methods to reuse the optical power link for transmitting slow control data. One low-power option is to add a liquid crystal modulator (LCM) as a variable attenuator in front of the PV cell. In this approach, the data to be transmitted is used to control LCM attenuation and thus modulate the amount of reflected light. The latter can be detected at the source end of the link by an auxiliary photodiode (PD). The maximum data rate of such a backscatter link, while limited by the relatively slow switching rate of the LCM, may still be fast enough for this application.

6 Development Plan and Milestones

The proposed timeline for completing the tasks described in Section 5 is shown in Table 2. Intermediate milestones are listed below:

- **Milestone 1 (month 3):** Fabrication and electrical testing of a flexible PCB for testing optical data and power links (Task 1) completed.
- **Milestone 2 (month 7):** Radiation testing of the flexible PCB (Task 2) completed.
- **Milestone 3 (month 10):** Design and simulation of a complete PIC-based EOM (including biasing and temperature control loop if needed, Tasks 4-6) completed.

7 Project Deliverables

The key project deliverables are summarized below for the following budget scenarios:

- **Scenario 1**: Realistic nominal budget (baseline budget).
- **Scenario 2**: Nominal budget minus 20%.
- **Scenario 3**: Nominal budget minus 40%.

The scope of the deliverables is limited to an initial demonstration of the feasibility of the proposed research tasks (Tasks 1-7). Further development of these tasks requires additional funding and will be pursued as part of follow-up projects.

Deliverable	**Scenario 1**	**Scenario 2**	**Scenario 3**
Fabrication of flexible PCB for optical data and power link testing	Month 2	Month 3	Month 4
Electrical test report of flexible PCB	Month 3	Month 4	Month 6
Radiation test report of flexible PCB	Month 7	Month 10	Month 12
Complete design of PIC-based EOM	Month 10	Month 12	N/A
Conceptual design and simulation of optically-isolated slow control link	Month 12	N/A	N/A

8 Resources and Budget

The *money matrix* for the project, which itemizes the budget allocations to the individual institutions, is shown below. Budget numbers are shown for the baseline case (Scenario 1).

Institution	**R&D Project**	**Budget**
Brookhaven National Laboratory (BNL)	Optical data & power links	$135,000
Lawrence Berkeley National Laboratory (LBNL)	Optical data & power links	$15,000

The detailed proposal budget is shown on the following pages. Three versions are shown, corresponding to budget Scenarios 1, 2, and 3, respectively.

Brookhaven National Laboratory

Directorate: *Director, Advanced Technology Research Office*
Department: *Instrumentation Division*
Title: *PHOTONICS-BASED READOUT AND POWER DELIVERY BY LIGHT FOR LARGE-AREA MONOLITHIC ACTIVE PIXEL SENSORS*
PIMS#: *7119*
Principal Investigator: *MANDAL,SOUMYAJIT*
Period of Performance: *10/1/2023 - 9/30/2024*
Sponsor: *DEPARTMENT OF ENERGY*
Project Rate Type: *IOR DOE & OLABS*

Sum of Amount			Reporting Year	
Cost Type	Group Break Descr	Descr	2024	Grand Total
Direct Costs	BNL Direct Labor	Base Labor	$ 58,850	$ 58,850
	BNL Direct Labor Total		$ 58,850	$ 58,850
	Materials and Supplies	PO Purchases	$ 20,520	$ 20,520
	Materials and Supplies Total		$ 20,520	$ 20,520
	Contract - High Value (Subcontract to LBNL)	Service Contract-High Value	$ 15,000	$ 15,000
	Contract - High Value (Subcontract to LBNL) Total		$ 15,000	$ 15,000
	Procurement Burden		$ 2,486	$ 2,486
	Departmental Charges		$ 9,557	$ 9,557
Direct Costs Total			**$ 106,413**	**$ 106,413**
Indirect Costs	Indirect Overheads-Project G&A	VAB Common Institutional Recov	$ 31,170	$ 31,170
		VAB G&A Recovery	$ 7,345	$ 7,345
	Indirect Overheads-Project G&A Total		$ 38,514	$ 38,514
	Indirect Overheads - LDRD		$ 5,072	$ 5,072
Indirect Costs Total			**$ 43,587**	**$ 43,587**
Grand Total			**$ 150,000**	**$ 150,000**

Sum of FTE		Reporting Year	
LaborType	Name	2024	Grand Total
SCIENTIFIC	MAJ,PIOTR G	0.03	0.03
	MANDAL,SOUMYAJIT	0.05	0.05
	RESCIA,SERGIO	0.05	0.05
	DEPTUCH,GRZEGORZ W	0.02	0.02
	ASCHENAUER,ELKE C	0.02	0.02
PROFESSIONAL	ST. JOHN,NICHOLAS B	0.05	0.05
	DEMINO,LEO J	0.03	0.03
OTHER	CARINI,GABRIELLA	0.01	0.01
Grand Total		**0.25**	**0.25**

Sum of Hours		Reporting Year	
LaborType	Name	2024	Grand Total
SCIENTIFIC	MAJ,PIOTR G	55	55
	MANDAL,SOUMYAJIT	81	81
	RESCIA,SERGIO	81	81
	DEPTUCH,GRZEGORZ W	31	31
	ASCHENAUER,ELKE C	31	31
PROFESSIONAL	ST. JOHN,NICHOLAS B	94	94
	DEMINO,LEO J	49	49
OTHER	CARINI,GABRIELLA	25	25
Grand Total		**448**	**448**

Sum of Months		Reporting Year	
LaborType	Name	2024	Grand Total
SCIENTIFIC	MAJ,PIOTR G	0.36	0.36
	MANDAL,SOUMYAJIT	0.55	0.55
	RESCIA,SERGIO	0.55	0.55
	DEPTUCH,GRZEGORZ W	0.21	0.21
	ASCHENAUER,ELKE C	0.21	0.21
PROFESSIONAL	ST. JOHN,NICHOLAS B	0.62	0.62
	DEMINO,LEO J	0.34	0.34
OTHER	CARINI,GABRIELLA	0.17	0.17
Grand Total		**2.99**	**2.99**

Brookhaven National Laboratory

Directorate: *Director, Advanced Technology Research Office*
Department: *Instrumentation Division*
Title: *PHOTONICS-BASED READOUT AND POWER DELIVERY BY LIGHT FOR LARGE-AREA MONOLITHIC ACTIVE PIXEL SENSORS*
PIMS#: *7119 - 20% Cut*
Principal Investigator: *MANDAL,SOUMYAJIT*
Period of Performance: *10/1/2023 - 9/30/2024*
Sponsor: *DEPARTMENT OF ENERGY*
Project Rate Type: *IOR DOE & OLABS*

Sum of Amount			Reporting Year	
Cost Type	Group Break Descr	Descr	2024	Grand Total
Direct Costs	BNL Direct Labor	Base Labor	$ 47,080	$ 47,080
	BNL Direct Labor Total		$ 47,080	$ 47,080
	Materials and Supplies	PO Purchases	$ 16,416	$ 16,416
	Materials and Supplies Total		$ 16,416	$ 16,416
	Contract - High Value (Subcontract to LBNL)	Service Contract-High Value	$ 12,000	$ 12,000
	Contract - High Value (Subcontract to LBNL) Total		$ 12,000	$ 12,000
	Procurement Burden		$ 1,989	$ 1,989
	Departmental Charges		$ 7,646	$ 7,646
Direct Costs Total			**$ 85,131**	**$ 85,131**
Indirect Costs	Indirect Overheads-Project G&A	VAB Common Institutional Recov	$ 24,936	$ 24,936
		VAB G&A Recovery	$ 5,876	$ 5,876
	Indirect Overheads-Project G&A Total		$ 30,812	$ 30,812
	Indirect Overheads - LDRD		$ 4,058	$ 4,058
Indirect Costs Total			**$ 34,869**	**$ 34,869**
Grand Total			**$ 120,000**	**$ 120,000**

Sum of FTE		Reporting Year	
LaborType	Name	2024	Grand Total
SCIENTIFIC	MAJ,PIOTR G	0.02	0.02
	MANDAL,SOUMYAJIT	0.04	0.04
	RESCIA,SERGIO	0.04	0.04
	DEPTUCH,GRZEGORZ W	0.01	0.01
	ASCHENAUER,ELKE C	0.01	0.01
PROFESSIONAL	ST. JOHN,NICHOLAS B	0.04	0.04
	DEMINO,LEO J	0.02	0.02
OTHER	CARINI,GABRIELLA	0.01	0.01
Grand Total		**0.20**	**0.20**

Sum of Hours		Reporting Year	
LaborType	Name	2024	Grand Total
SCIENTIFIC	MAJ,PIOTR G	44	44
	MANDAL,SOUMYAJIT	65	65
	RESCIA,SERGIO	65	65
	DEPTUCH,GRZEGORZ W	25	25
	ASCHENAUER,ELKE C	25	25
PROFESSIONAL	ST. JOHN,NICHOLAS B	75	75
	DEMINO,LEO J	39	39
OTHER	CARINI,GABRIELLA	20	20
Grand Total		**358**	**358**

Sum of Months		Reporting Year	
LaborType	Name	2024	Grand Total
SCIENTIFIC	MAJ,PIOTR G	0.29	0.29
	MANDAL,SOUMYAJIT	0.44	0.44
	RESCIA,SERGIO	0.44	0.44
	DEPTUCH,GRZEGORZ W	0.17	0.17
	ASCHENAUER,ELKE C	0.17	0.17
PROFESSIONAL	ST. JOHN,NICHOLAS B	0.50	0.50
	DEMINO,LEO J	0.27	0.27
OTHER	CARINI,GABRIELLA	0.13	0.13
Grand Total		**2.39**	**2.39**

Brookhaven National Laboratory

Directorate: *Director, Advanced Technology Research Office*
Department: *Instrumentation Division*
Title: *PHOTONICS-BASED READOUT AND POWER DELIVERY BY LIGHT FOR LARGE-AREA MONOLITHIC ACTIVE PIXEL SENSORS*
PIMS#: *7119 - 40% Cut*
Principal Investigator: *MANDAL,SOUMYAJIT*
Period of Performance: *10/1/2023 - 9/30/2024*
Sponsor: *DEPARTMENT OF ENERGY*
Project Rate Type: *IOR DOE & OLABS*

Sum of Amount			Reporting Year	
Cost Type	Group Break Descr	Descr	2024	Grand Total
Direct Costs	BNL Direct Labor	Base Labor	$ 35,310	$ 35,310
	BNL Direct Labor Total		$ 35,310	$ 35,310
	Materials and Supplies	PO Purchases	$ 12,312	$ 12,312
	Materials and Supplies Total		$ 12,312	$ 12,312
	Contract - High Value (Subcontract to LBNL)	Service Contract-High Value	$ 9,000	$ 9,000
	Contract - High Value (Subcontract to LBNL) Total		$ 9,000	$ 9,000
	Procurement Burden		$ 1,492	$ 1,492
	Departmental Charges		$ 5,734	$ 5,734
Direct Costs Total			**$ 63,848**	**$ 63,848**
Indirect Costs	Indirect Overheads-Project G&A	VAB Common Institutional Recov	$ 18,702	$ 18,702
		VAB G&A Recovery	$ 4,407	$ 4,407
	Indirect Overheads-Project G&A Total		$ 23,109	$ 23,109
	Indirect Overheads - LDRD		$ 3,043	$ 3,043
Indirect Costs Total			**$ 26,152**	**$ 26,152**
Grand Total			**$ 90,000**	**$ 90,000**

Sum of FTE		Reporting Year	
LaborType	Name	2024	Grand Total
SCIENTIFIC	MAJ,PIOTR G	0.02	0.02
	MANDAL,SOUMYAJIT	0.03	0.03
	RESCIA,SERGIO	0.03	0.03
	DEPTUCH,GRZEGORZ W	0.01	0.01
	ASCHENAUER,ELKE C	0.01	0.01
PROFESSIONAL	ST. JOHN,NICHOLAS B	0.03	0.03
	DEMINO,LEO J	0.02	0.02
OTHER	CARINI,GABRIELLA	0.01	0.01
Grand Total		**0.15**	**0.15**

Sum of Hours		Reporting Year	
LaborType	Name	2024	Grand Total
SCIENTIFIC	MAJ,PIOTR G	33	33
	MANDAL,SOUMYAJIT	49	49
	RESCIA,SERGIO	49	49
	DEPTUCH,GRZEGORZ W	19	19
	ASCHENAUER,ELKE C	19	19
PROFESSIONAL	ST. JOHN,NICHOLAS B	56	56
	DEMINO,LEO J	29	29
OTHER	CARINI,GABRIELLA	15	15
Grand Total		**269**	**269**

Sum of Months		Reporting Year	
LaborType	Name	2024	Grand Total
SCIENTIFIC	MAJ,PIOTR G	0.22	0.22
	MANDAL,SOUMYAJIT	0.33	0.33
	RESCIA,SERGIO	0.33	0.33
	DEPTUCH,GRZEGORZ W	0.13	0.13
	ASCHENAUER,ELKE C	0.13	0.13
PROFESSIONAL	ST. JOHN,NICHOLAS B	0.37	0.37
	DEMINO,LEO J	0.20	0.20
OTHER	CARINI,GABRIELLA	0.10	0.10
Grand Total		**1.79**	**1.79**

References

[1] R. Abdul Khalek et al. "Science Requirements and Detector Concepts for the Electron-Ion Collider: EIC Yellow Report". In: *Nuclear Physics A* 1026 (2022), p. 122447. ISSN: 0375-9474. DOI: https://doi.org/10.1016/j.nuclphysa.2022.122447. URL: https://www.sciencedirect.com/science/article/pii/S0375947422000677.

[2] ATLAS LAr Collaboration. "Optical Links for ATLAS liquid argon calorimeter front-end electronics readout". In: *Journal of Instrumentation* 6.01 (2011), p. C01013.

[3] C Bauer, R Frei, A Vollhardt, D Esperanto, U Straumann, and P Vázquez. *Grounding, shielding and power distribution for the LHCb silicon tracking*. Tech. rep. 2005.

[4] Boualem Bendib, Hocine Belmili, and Fateh Krim. "A survey of the most used MPPT methods: Conventional and advanced algorithms applied for photovoltaic systems". In: *Renewable and Sustainable Energy Reviews* 45 (2015), pp. 637–648.

[5] Vincent Bobillier, R Frei, and J Christiansen. *Grounding, Shielding and Power Distribution in LHCb*. Tech. rep. CERN-LHCb-2004-039, 2004.

[6] Guangwei Cong, Yuriko Maegami, Morifumi Ohno, and Koji Yamada. "Ultra-compact non-travelling-wave silicon carrier-depletion Mach-Zehnder modulators towards high channel density integration". In: *IEEE Journal of Selected Topics in Quantum Electronics* 27.3 (2020), pp. 1–11.

[7] G. Deptuch, J.-D. Berst, G. Claus, C. Colledani, W. Dulinski, Y. Gornushkin, D. Husson, J.-L. Riester, and M. Winter. "Design and testing of monolithic active pixel sensors for charged particle tracking". In: *IEEE Transactions on Nuclear Science* 49.2 (2002), pp. 601–610. DOI: 10.1109/TNS.2002.1003683.

[8] Mohamed A Eltawil and Zhengming Zhao. "MPPT techniques for photovoltaic applications". In: *Renewable and sustainable energy reviews* 25 (2013), pp. 793–813.

[9] D.S. Gorni, G.W. Deptuch, S. Miryala, D.P. Siddons, A. Kuczewski, A.K. Rumaiz, and G.A. Carini. "Event driven readout architecture with non-priority arbitration for radiation detectors". In: *Journal of Instrumentation* 17.04 (Apr. 2022), p. C04027. DOI: 10.1088/1748-0221/17/04/C04027. URL: https://dx.doi.org/10.1088/1748-0221/17/04/C04027.

[10] L. Greiner et al. "A MAPS based vertex detector for the STAR experiment at RHIC". In: *Nuclear Instruments and Methods in Physics Research Section A: Accelerators, Spectrometers, Detectors and Associated Equipment* 650.1 (2011). International Workshop on Semiconductor Pixel Detectors for Particles and Imaging 2010, pp. 68–72. ISSN: 0168-9002. DOI: https://doi.org/10.1016/j.nima.2010.12.006. URL: https://www.sciencedirect.com/science/article/pii/S0168900210027439.

[11] Andrea Kraxner, Stephane Detraz, Lauri Olantera, Carmelo Scarcella, Christophe Sigaud, Csaba Soos, Jan Troska, and Francois Vasey. "Investigation of the influence of temperature and annealing on the radiation hardness of silicon Mach–Zehnder modulators". In: *IEEE Transactions on Nuclear Science* 65.8 (2018), pp. 1624–1631.

[12] Howard S Matis, Ralph L Brown, William Christie, WR Edwards, Richard Jared, Bob Minor, and Paul Salz. "Integration and conventional systems at STAR". In: *Nuclear Instruments and Methods in Physics Research Section A: Accelerators, Spectrometers, Detectors and Associated Equipment* 499.2-3 (2003), pp. 802–813.

[13] P Moreira, T Toifl, A Kluge, G Cervelli, F Faccio, A Marchioro, and J Christiansen. "G-Link and Gigabit Ethernet compliant serializer for LHC data transmission". In: *2000 IEEE Nuclear Science Symposium. Conference Record (Cat. No. 00CH37149)*. Vol. 2. IEEE. 2000, pp. 9–6.

[14] Paulo Moreira, K Wyllie, B Yu, A Marchioro, C Paillard, K Kloukinas, T Fedorov, N Pinilla, R Ballabriga, S Bonacini, et al. "The GBT project". In: (2009).

[15] F. Piro et al. "A 1-μW Radiation-Hard Front-End in a 0.18-μm CMOS Process for the MALTA2 Monolithic Sensor". In: *IEEE Transactions on Nuclear Science* 69.6 (2022), pp. 1299–1309. DOI: 10.1109/TNS.2022.3170729.

[16] Theoni Prousalidi, A Bulling, S Detraz, M Lalović, L Marcon, L Olanterä, S Orfanelli, U Sandven, C Scarcella, C Sigaud, et al. "Towards optical data transmission for high energy physics using silicon photonics". In: *Journal of Instrumentation* 17.05 (2022), p. C05004.

[17] Michal Rakowski, Colleen Meagher, Karen Nummy, Abdelsalam Aboketaf, Javier Ayala, Yusheng Bian, Brendan Harris, Kate Mclean, Kevin McStay, Asli Sahin, et al. "45nm CMOS-silicon photonics monolithic technology (45CLO) for next-generation, low power and high speed optical interconnects". In: *Optical Fiber Communication Conference*. Optica Publishing Group. 2020, T3H–3.

[18] W. Snoeys. "Monolithic pixel detectors for high energy physics". In: *Nuclear Instruments and Methods in Physics Research Section A: Accelerators, Spectrometers, Detectors and Associated Equipment* 731 (2013). PIXEL 2012, pp. 125–130. ISSN: 0168-9002. DOI: https://doi.org/10.1016/j.nima.2013.05.073. URL: https://www.sciencedirect.com/science/article/pii/S0168900213006840.

[19] W. Snoeys et al. "A process modification for CMOS monolithic active pixel sensors for enhanced depletion, timing performance and radiation tolerance". In: *Nuclear Instruments and Methods in Physics Research Section A: Accelerators, Spectrometers, Detectors and Associated Equipment* 871 (2017), pp. 90–96. ISSN: 0168-9002. DOI: https://doi.org/10.1016/j.nima.2017.07.046. URL: https://www.sciencedirect.com/science/article/pii/S016890021730791X.

[20] Walter Snoeys. "How chips helped discover the Higgs boson at CERN". In: *2014 44th European Solid State Device Research Conference (ESSDERC)*. IEEE. 2014, pp. 9–19.

[21] Jan Troska, François Vasey, and Anthony Weidberg. "Radiation tolerant optoelectronics for high energy physics". In: *Nuclear Instruments and Methods in Physics Research Section A: Accelerators, Spectrometers, Detectors and Associated Equipment* (2023), p. 168208.

[22] Le Xiao, Xiaoting Li, Datao Gong, Jinghong Chen, Di Guo, Huiqin He, Suen Hou, Guangming Huang, Chonghan Liu, Tiankuan Liu, et al. "LOCx2, a low-latency, low-overhead, 2$\times$ 5.12-Gbps transmitter ASIC for the ATLAS Liquid Argon Calorimeter trigger upgrade". In: *Journal of Instrumentation* 11.02 (2016), p. C02013.

[23] P. Yang et al. "Low-power priority Address-Encoder and Reset-Decoder data-driven readout for Monolithic Active Pixel Sensors for tracker system". In: *Nuclear Instruments and Methods in Physics Research Section A: Accelerators, Spectrometers, Detectors and Associated Equipment* 785 (2015), pp. 61–69. ISSN: 0168-9002. DOI: https://doi.org/10.1016/j.nima.2015.02.063. URL: https://www.sciencedirect.com/science/article/pii/S0168900215002818.